INTERNATIONAL JOURNAL FOR NUMERICAL METHODS IN FLUIDS
Int. J. Numer. Meth. Fluids 2000; **33**: 475–498

Numerical simulation and analysis of three-dimensional turbulent impinging square twin-jet flow field with no-crossflow

Shu-Hao Chuang* and Tsu-Jui Nieh

Institute of Mechanical Engineering, National Chung-Hsing University, Taichung, Taiwan, Republic of China

SUMMARY

The three-dimensional turbulent impinging square twin-jet flow with no-crossflow is analyzed by employing the computational fluid dynamics (CFD) code PHOENICS. The SIMPLEST algorithm and the Jones–Launder k–ε two-equation turbulence model are used to simulate the strong turbulence of the three-dimensional impinging twin-jet flow field. The transport properties of velocity, pressure, and structure of exhausted nozzles at a space of $S = 5D$, jet exit height of $H = 3D$, and main nozzle jet Reynolds number of 105000 are solved in this paper. The axial velocities of the present calculated results are found to be in good agreement with the experimental data of Barata *et al.* [Barata JMM, Durao DFG, Heitor MV. Impingement of single and twin turbulent jets through a crossflow. *AIAA Journal* 1991; **29**: 595–602]. The calculated results show that the flow field structure of twin-jet impinging on a flat surface is strongly affected by the depth of geometry. Also, the calculated results show that several recirculating zones are distributed around the flow field. Their size and location are different from the two-dimensional flow field due to the effect of flow stretching in the y-direction. In addition, fountain upwash flow is extended to the narrow region of the outer boundary. The phenomena in the present analysis provide a fundamental numerical study of three-dimensional impinging twin-jet flow fields and a basis for the further analysis of three-dimensional impinging twin-jet flow fields with a variable angle nozzle and plate. Copyright © 2000 John Wiley & Sons, Ltd.

KEY WORDS: fountain upwash flow; no-crossflow; recirculation zone; three-dimensional turbulent flow; twin-jet impinging flow

1. INTRODUCTION

The structural analysis of the impinging jet is very important because of its wide application to engineering and practical problems, such as dryers, annealing of metal and glass, forming of plastic, secondary cooling of cast iron, cooling of transistors, cooling of turbine blades, drying of textile and paper, heating of glass products, the take-off of V/STOL aircraft (as

* Correspondence to: Institute of Mechanical Engineering, National Chung-Hsing University, 250 Kuo-Kuang Road, Taichung, Taiwan 402, Republic of China.

Received November 1998
Revised March 1999

shown in Figure 1), and the vectoring of fighter planes. Studies of a three-dimensional impinging twin-jet flow may provide some basic understanding of the practical three-dimensional multiple impinging jets flow field. The effects of ground plane on impinging jet flow are important to the performance of V/STOL aircraft design. The three-dimensional vectored jet impinging on the ground plane and the wall jet flow field developed along the downstream ground plane between the twin-jet are very complicated phenomena. To approach these phenomena using theoretical analysis or experimental measurements can be quite difficult. The cost of experimentation may be substantial in order to understand the structure of the impinging twin-jet flow field. Therefore, numerical simulation may be a cost-effective approach to the investigation of an impinging twin-jet flow field. Three-dimensional impinging twin-jet flow fields can be divided into ten regions: (1) free jet region, (2) jet impingement region, (3) lower wall jet region, (4) fountain formation region, (5) fountain up-wash region, (6) combined wall jet region, (7) stagnation line region, (8) fountain impingement region, (9) upper wall jet region, (10) entrainment region (as shown in Figures 2 and 3). Their structures are somewhat different from the two-dimensional impinging jet [1,2] and twin-jet [3].

1.1. Review papers of two-dimensional impinging jet and twin-jet flow

Wolfshtein [4] summarized all experimental and analytic studies of the planar turbulent impinging jet up to 1970 in his review paper. Experimental measurements of the impinging jet with a round nozzle were carried out by Coleman [5], who found that the flow was essentially characterized by three regions, namely the free jet region, the jet impingement region, and the wall jet region. The static pressure distribution of the ground plane for the impinging region has been solved by the frozen vorticity concept [6]. Theoretical analyses of impinging jet flow have been concerned with finding solutions of several separate regions and then combining these into a complete solution [7,8]. The two-dimensional Navier–Stokes equation with ground effect was studied by Bower and Kotansky [9], who first utilized the augmented central difference and the one-equation turbulent model to simulate the impinging jet flow. A two-dimensional impinging jet flow was studied by Bower and co-workers [10,11], who utilized the streamfunction–vorticity and Jones–Launder [12] k–ε two-equation turbulence models.

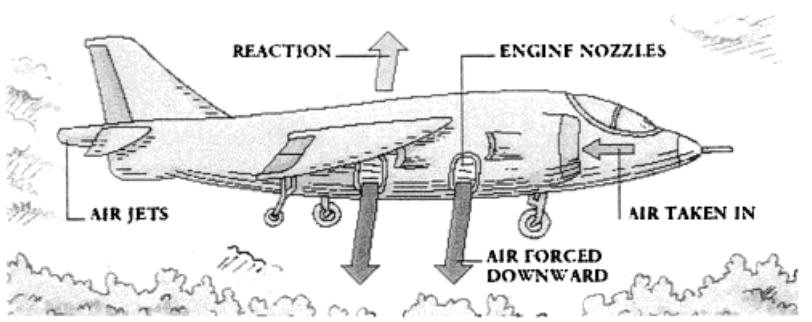

Figure 1. V/STOL military aircraft.

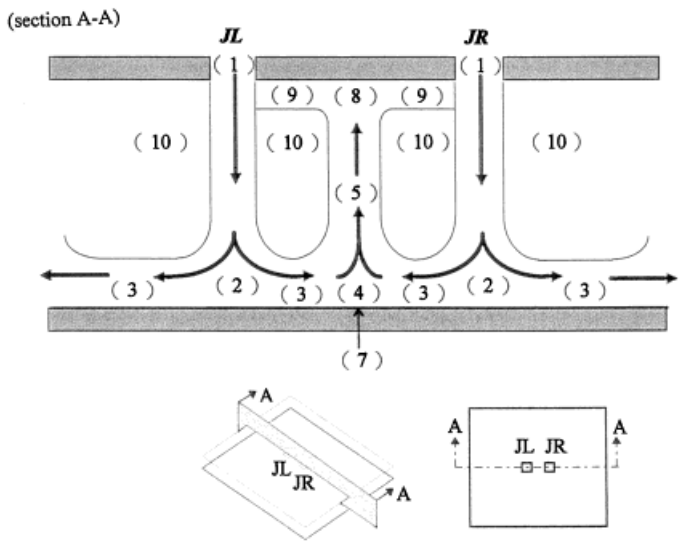

Figure 2. Impinging twin jet flow structure of central plane across two exhaust nozzles.

These results showed good agreement between numerical predictions and experimental data. Incompressible, inviscid, rotational impingement problems have also been considered [13]. The results for two-dimensional normal axisymmetric impingement and oblique impingement jets compared well with the experimental data of Rubel [13]. Agarwal and Bower [14] and Looney and Walsh [15] used the same turbulence model to predict the impinging jet flow and found similar agreement. The above solution methods were limited to the use of the streamfunction–vorticity for solving the Navier–Stokes equations. Ho and Nosseir [16] investigated the feedback phenomenon in an impinging jet. They found that pressure fluctuations were generated by the impingement of the coherent structures on the plate. Besides, these pressure fluctuations will induce self-sustained oscillations in some situations [17,18]. Ho and Hsiao [19] employed an experimental method to study the interaction between the free shear layer and the boundary layer of the wall jet. In order to further understand the structure of impinging jet flow, one needs to use the primitive variables for solving an impinging twin-jet flow. In viscous flow the fine mesh spacing makes the MacCormack scheme with the explicit method [20,21] extremely costly. Implicit methods [22,23] make use of a possible large time step but require the inversion of block tridiagonal matrices. A numerical simulation of impinging jet flow using the Beam–Warming method [22] has been performed by Hwang and Liu [24]. A method developed by MacCormack [25] has eliminated this disadvantage by introducing a predictor–corrector scheme. Unfortunately, this method was demonstrated only for a simple case. There are some studies [1–3,26–31] of impinging single-jet and twin-jet flows showing good agreement between numerical predictions and experimental data. Miller [32] employed an experimental method to measure the flow properties of wall jets resulting from single and multiple inclined round jet impingement in a two-dimensional flow. Seyedein *et al.* [33] used

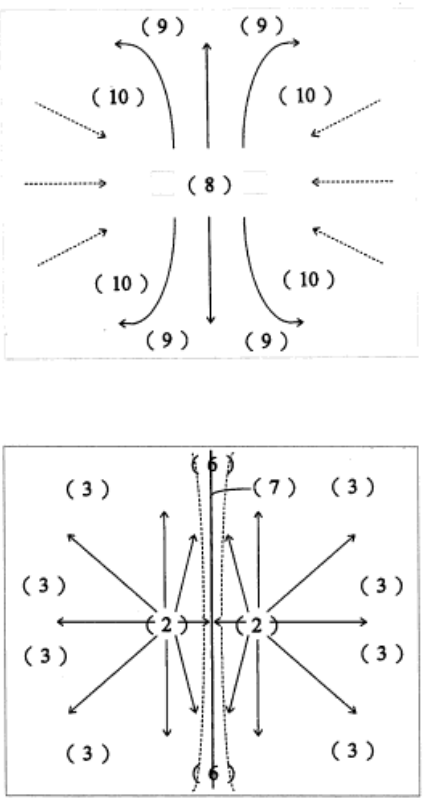

Figure 3. Schematic flow structure of three-dimensional impinging twin jet. (a) Flow structure of upper plate, (b) flow structure of lower plate.

the numerical method to simulate the two-dimensional turbulent flow and heat transfer from confined multiple impinging slot jets. Their calculated results show that the predicted value of the Lam–Bremhorst low-Reynolds number model is prior to the standard high-Reynolds number model.

1.2. Review papers of three-dimensional impinging jet and twin-jet flow

Experimental measurements with the pitot tube of the three-dimensional impinging jet with a round nozzle with various impinging surfaces, such as plane, convex, concave, and cylinder, were carried out by Donaldson and Snedeker [34]. Siclari *et al*. [8] had calculated the results of theoretical models for three-dimensional jet-induced effects on V/STOL aircraft. Siclari *et al*. [35] employed an experimental method to study the three-dimensional two-impinging jets

flow, the main purpose of this study is concentrated in the stagnation line and up-wash formation. A three-dimensional impinging jet flow with a rectangular nozzle was studied by Kotansky and Glaze [36], who used an experimental method approach. Elbanna and Gahin [37] used an experimental method to investigate the two-plane parallel jets; the measured properties are the main velocity, the turbulent intensity, and Reynolds shear stress. A numerical study of three-dimensional single impinging jet with crossflow was performed by Barata *et al*. [38]. Their numerical schemes included Hybrid and QUICK schemes. McGuirk *et al*. [39] employed experimental and numerical methods to investigate the three-dimensional impinging round jet flow with crossflow. Their algorithm models are a low-order Hybrid scheme and a high-order QUICK scheme. A three-dimensional turbulent flow of hot gas ingestion was studied by Vanoverbeke and Holdeman [40], who used the TEACH-type code. Yoo and Strash [41] employed the three codes VSAERO, ARC3D, and APPL to calculate and simulate a three-dimensional V/STOL aerodynamics flow. The impingement of single and twin turbulent jets through a crossflow was studied by Durao *et al*. [42], who employed a Laser–Doppler device to measure the flow properties and used a QUICK scheme to finish the numerical method. Experimental measurements with the split-film probe of the three-dimensional impinging parallel jets flow were carried out by Lin and co-workers [43,44]. They found that the interaction flow between jets can be divided into three regions, such as the converging region, the merging region, and the combined region. Tafti and Vanka [45] employed the code of full multigrid cycle to solve the k–ε two-equation and simulate the hot gas environment around V/STOL aircraft. Also, Roth *et al*. [46] employed the code F3D with implicit, two-factor, partial flux splitting method to solve the thin-layer of the Navier–Stokes equation of the three-dimensional impinging compressible flow with crossflow. Kim and Benson [47,48] employed the M-S model to simulate the three-dimensional impinging jets and multiple jets with crossflow. They proved that good results for non-equilibrium turbulent flow can be obtained using the M-S model. Experimental measurements of three-dimensional impinging axisymmetric jet flow at various nozzle angles were carried out by Özdemirc and Whitelaw [49].

The jet impinging on the ground plane and the wall jet flow field that develop downstream of the ground plane are very complicated phenomena. The lift force is produced by the jet propulsion force and the ground effect. The jets, in general, come from the engine exhaust gas, which is a high-temperature, high-pressure gas. In this environment, the surrounding fluid is induced by the impinging jets and made form recirculations. Then, the up-wash fountain flow is formed between the twin-jet. The above review papers are summarized in Table I. According to Table I, studies of three-dimensional impinging twin-jet flow with square nozzles are scarce. Therefore, the intention of this paper is to investigate the phenomena of a three-dimensional impinging square twin-jet flow field with no-crossflow. This paper employed the code PHOENICS and adopted the SIMPLEST algorithm and the Jones–Launder k–ε two-equation turbulence model. The finite difference equations are derived by integrating the governing equations over a control volume surrounding each grid point. A hybrid scheme [50] is used for the representation of the connective and diffusive terms across the control surface.

Table I. Arrangement of references.

Reference number	Experimental	Numerical	2D	3D	1J	2J	Multi-J	Round	Square	Slot	Crossflow
[8]		*		*		*	*	*			
[26]		*	*			*				*	
[27]		*	*			*				*	*
[28]		*	*			*				*	
[29]		*	*			*				*	*
[30]		*	*			*				*	*
[31]		*	*			*				*	*
[32]	*		*		*	*	*	*			
[33]		*	*				*			*	
[34]	*			*	*			*			
[35]	*	*		*		*		*			
[36]	*	*		*	*				*		
[37]	*			*		*				*	
[38]		*		*	*			*			*
[39]	*	*		*	*			*			
[40]		*		*		*			*		*
[41]		*		*	*			*			*
[42]	*	*		*	*	*		*			*
[43]	*			*		*				*	
[44]	*			*		*		*			
[45]		*		*		*			*		*
[46]		*		*	*			*			*
[47]		*		*	*			*			*
[48]		*		*			*	*			*
[49]	*			*	*			*			
[50]											
[51]											
[52]											

2. THEORETICAL MODEL

2.1. Physical model

The basic configuration of the numerical simulation region is shown in Figure 4. The top view and front view of the physical model are shown in Figures 5 and 6 respectively. Both sizes of the nozzles are $D \times D$, and the space between the exhaust nozzles and the dimension of the plates are S and $(30D + S) \times 30D$, as shown in Figure 5. The height of the jet exit plane above ground is H, and the exit velocity of the nozzle is V_j. In this paper, in order to show the quality analysis of three-dimensional impinging twin-jet flow with two square nozzles, we let $S = 5D$, $H = 3D$, and $Re_{V_j} = 105000$, where $V_j = 16.212$ m s^{-1}. The grid points used here are $84 \times 70 \times 12$ in the x-, y-, and z-directions respectively.

2.2. Assumptions

In order to simplify the three-dimensional impinging twin-jet flow, the following assumptions are made:

1. the fluid is a Newton viscous fluid and incompressible flow
2. the flow is turbulent and steady state
3. gravity effects are negligible
4. isotropic turbulent flow is considered
5. the flow is isothermal
6. the jets flow from the nozzle are uniform

2.3. Governing equations

For the steady three-dimensional turbulent impinging twin-jet flow, the transport equation with rectangular co-ordinates can be written as

Continuity equation

$$\frac{\partial u_i}{\partial x_i} = 0 \tag{1}$$

Navier–Stokes equation

$$\frac{\partial (u_i u_j)}{\partial x_j} = -\frac{1}{\rho}\frac{\partial p}{\partial x_j} + \nu \frac{\partial}{\partial x_j}\left[\frac{\partial u_i}{\partial x_j} + \frac{\partial u_j}{\partial x_i}\right] \tag{2}$$

where u_i is the velocity component in the i-direction, $i = 1, 2, 3$. The required grid number of the Navier–Stokes equation is very large if we directly solve the problem with numerical analysis. In order to simplify the grid system of the impinging twin-jet flow, the k–ε [12] turbulent model is used to simulate the three-dimensional turbulent flow. Now, the governing equations are obtained as

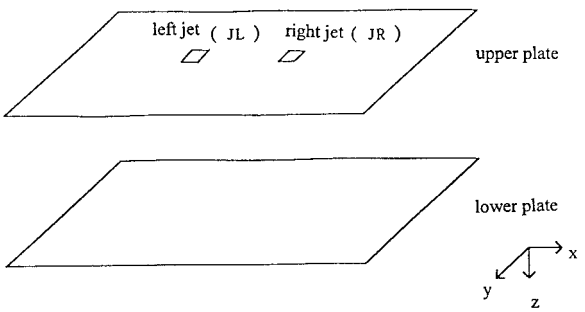

Figure 4. Physical configuration of three-dimensional impinging twin-jet.

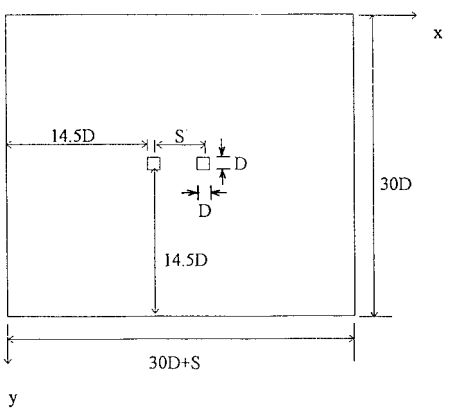

Figure 5. Top view of physical configuration.

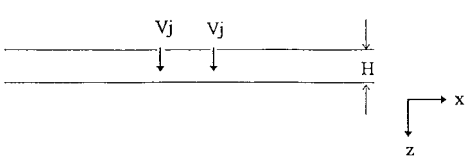

Figure 6. Front view of physical configuration.

Continuity equation

$$\frac{\partial \bar{u}_i}{\partial x_i} = 0 \tag{3}$$

Navier–Stokes equation

$$\frac{\overline{\partial (u_i u_j)}}{\partial x_j} = -\frac{\partial}{\partial x_j}\left(\frac{\bar{P}}{\rho} + \frac{2}{3}k\right) + \frac{\partial}{\partial x_j}\left[v_t\left(\frac{\partial \bar{u}_i}{\partial x_j} + \frac{\partial \bar{u}_j}{\partial x_i}\right)\right] \tag{4}$$

k transportation equation

$$\frac{\partial k\bar{u}_j}{\partial x_j} = \frac{\partial}{\partial x_j}\left(\frac{v_t}{\sigma_k}\frac{\partial k}{\partial x_j}\right) + v_t S - \varepsilon \tag{5}$$

ε transportation equation

$$\frac{\partial \varepsilon\bar{u}_j}{\partial x_j} = \frac{\partial}{\partial x_j}\left(\frac{v_t}{\sigma_\varepsilon}\frac{\partial \varepsilon}{\partial x_j}\right) + c_1\frac{\varepsilon}{k}v_t S - c_2\frac{\varepsilon^2}{k} \tag{6}$$

where

$u_i = \bar{u}_i + u_i'$, u_i' is a fluctuation velocity

$$S = \left(\frac{\partial \bar{u}_i}{\partial x_j} + \frac{\partial \bar{u}_j}{\partial x_i}\right)\frac{\partial \bar{u}_i}{\partial x_j}$$

$$v_t = c_\mu \frac{k^2}{\varepsilon}$$

$$k = \frac{1}{2}\overline{u_i' u_i'} = \frac{3}{2}I^2 U^2$$

$$\varepsilon = v\,\overline{\left(\frac{\partial u_i'}{\partial x_j}\right)^2} = \frac{c_\mu k^2}{v_t}$$

$$\overline{u_i' u_j'} = \frac{2}{3}k\delta_{ij} - v_t\left(\frac{\partial \bar{u}_i}{\partial x_j} + \frac{\partial \bar{u}_j}{\partial x_i}\right)$$

Launder and Spalding [51] suggested the constants of the coefficients used in the present study are $c_\mu = 0.09$, $c_1 = 1.44$, $c_2 = 1.92$, $\rho_k = 1.0$, $\rho_\varepsilon = 1.3$.

3. NUMERICAL ANALYSIS AND BOUNDARY CONDITIONS

3.1. Grid system

The numerical calculation domain and grids used are shown in Figure 7. The grid size at the twin-jet nozzles and the distance between the two nozzles are uniform in the x- and y-directions, and then expand downstream from the nozzle edge. Also the grid size is uniform in the z-direction.

The staggered grid arrangement of integration over the control volume was used to avoid wavy phenomena [50]. For the present problem, the arrangement of the grid system $84 \times 70 \times 12$ is optimum when checking the accuracy of grids and convergence rate, as shown in Figure 8.

3.2. Finite difference equations

The general form of Equations (3)–(6) for steady flow can be written as

$$\underbrace{\frac{\partial}{\partial x}(\phi u)+\frac{\partial}{\partial y}(\phi v)+\frac{\partial}{\partial z}(\phi w)}_{\text{Convection term}}=\underbrace{\frac{\partial}{\partial x}\left(\Gamma_\phi \frac{\partial \phi}{\partial x}\right)+\frac{\partial}{\partial y}\left(\Gamma_\phi \frac{\partial \phi}{\partial y}\right)+\frac{\partial}{\partial z}\left(\Gamma_\phi \frac{\partial \phi}{\partial z}\right)}_{\text{Diffusion term}}+\underbrace{S_\phi}_{\text{Source term}} \tag{7}$$

where ϕ denotes the dependent variables such as u, v, w, k, and ε. Γ_ϕ is the transfer coefficient of ϕ.

Integration over the control volume cell was employed to construct the finite difference equations. First, the general form of Equation (7) can be rewritten as

$$\frac{\partial J_x}{\partial x}+\frac{\partial J_y}{\partial y}+\frac{\partial J_z}{\partial z}=S_\phi \tag{8}$$

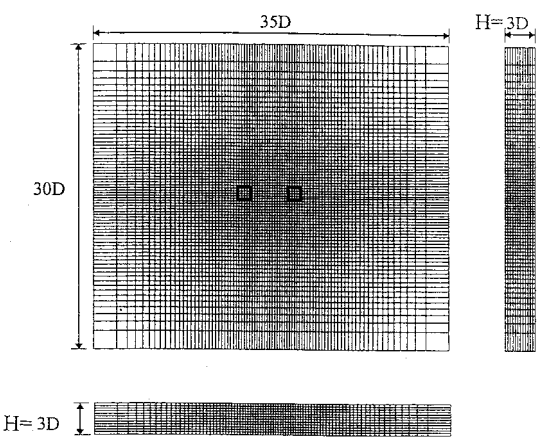

Figure 7. Grid system ($S = 5D$, $H = 3D$).

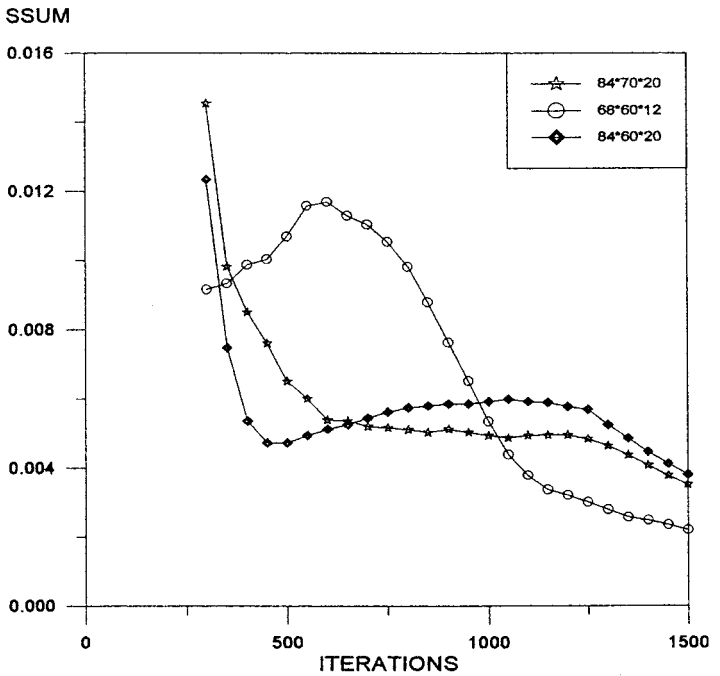

Figure 8. Test of the independence of grid points.

where

$$J_x = u\phi - \Gamma_\phi \frac{\partial \phi}{\partial x}$$

$$J_y = v\phi - \Gamma_\phi \frac{\partial \phi}{\partial y}$$

$$J_z = w\phi - \Gamma_\phi \frac{\partial \phi}{\partial z}$$

Integration of Equation (8) over the control volume gives

$$J_e - J_w + J_n - J_s + J_h - J_l = 0 \tag{9}$$

where the adopted control volume is shown in Figure 9, and J_i is the net total flux at control interface i. Also, integration of the continuity equation over the control volume cell gives

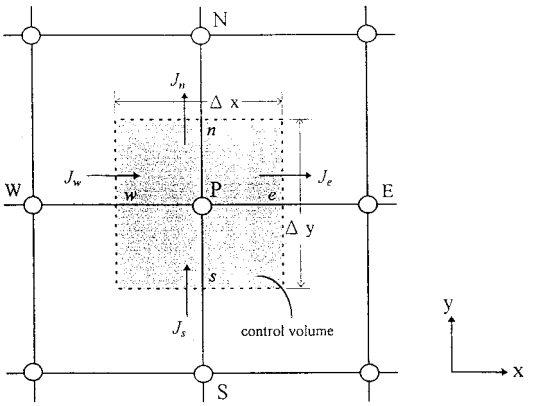

Figure 9. Control volume arrangement for x–y plane.

$$F_e - F_w + F_n - F_s + F_h - F_l = S_\phi \Delta x \Delta y \Delta z \tag{10}$$

where F_i is the mass flow rate at control interface i, which are the following:

$$F_e = u_e \Delta y \Delta z$$

$$F_w = u_w \Delta y \Delta z$$

$$F_n = v_n \Delta z \Delta x$$

$$F_s = v_s \Delta z \Delta x$$

$$F_h = w_h \Delta x \Delta y$$

$$F_l = w_l \Delta x \Delta y$$

Subtracting Equation (10) multiplied by ϕ_p from Equation (9) gives

$$(J_e - F_e\phi_p) - (J_w - F_w\phi_p) + (J_n - F_n\phi_p) - (J_s - F_s\phi_p) + (J_h - F_h\phi_p) - (J_l - F_l\phi_p) = S_\phi \Delta x \Delta y \Delta z \tag{11}$$

The source term needs to be linearized [50], such that $S_\phi = S_c + S_p\phi_p$. The Hybrid scheme [50] is used here. Then, the total flux of the control volume cell can be written as

$$J_i - F_i\phi_p = a_i(\phi_p - \phi_i), \quad i = \text{e, n, h}$$

$$J_i - F_i\phi_p = a_i(\phi_i - \phi_p), \quad i = \text{w, s, l} \tag{12}$$

where

$$a_i = D_i A(|P_i|) + [-F_i, 0], \quad i = \text{e, n, h}$$

$$a_i = D_i A(|P_i|) + [F_i, 0], \quad i = \text{w, s, l} \tag{13}$$

$A(|P_i|) = [0, 1 - 0.5|P_i|]$, $P_i = F_i/D_i$ is the Peclet number for surface i; $[A, B]$ means the choice of maximum value between A and B, and $D_i = \Gamma_i A_i/(\delta x)_i$. Substituting these relations into Equation (11), we obtain

$$a_p \phi_p = a_e \phi_e + a_w \phi_w + a_n \phi_n a_s \phi_s + a_h \phi_h + a_l \phi_l + b \tag{14}$$

where

$$b = S_c \Delta x \Delta y \Delta z$$

$$a_p = a_e + a_w + a_n + a_s + a_h + a_l - S_p \Delta x \Delta y \Delta z$$

3.3. Solution technique

The SIMPLEST [52] (SIMPLE short tend) algorithm was employed to solve the present problem. The SIMPLEST algorithm originates from the SIMPLE algorithm. The advantage of SIMPLEST is fast convergence. For a point n, the finite difference of the momentum equation is $a_n u_n = \Sigma (d_n u_n) + \Sigma (c_n u_n) + b$, where u is the velocity at point n, d is the diffusion coefficient, c is the convection coefficient, and b is the source term. The momentum finite difference equation is written as $a_n u_n = \Sigma (d_n + c_n) u_n + b$ when we use the SIMPLE algorithm. The momentum finite difference equation is written as $a_n u_n = \Sigma (d_n u_n) + (\Sigma (c_n u_n) + b)$ when we use the SIMPLEST algorithm. The convection effect is neglected for the SIMPLEST algorithm in order to increase the convergence rate. The solution procedure is aided and achieved by the code of PHOENICS (parabolic, hyperbolic or elliptic numerical integration code series). The flow chart of the numerical simulation is shown in Figure 10.

The structures of the PHOENICS code are included in two main codes SATELLITE and EARTH, and four auxiliary codes PHOTON, AUTOPLOT, PINTO, and GUIDE. The function of SATELLITE is the front treatment, EARTH is the main calculation, PHOTON, AUTOPLOT, and PINTO are the back treatment, and GUIDE is an auxiliary information. The solution procedures are initiated with estimates for the velocity and pressure fields and they then proceed with line-by-line iterations. After each sweep over the solution domain, adjustments for the pressure and velocity fields are made to satisfy the continuity equation along each line of the control volume. Iterations are continued until the continuity equation is satisfied to the convergence criterion. The tolerance of normalized mass residual is typically $\Sigma |R_\phi| < 10^{-3}$. The control processor time on a HP-9000/755 computer is about 12–20 h to convergence for 1500–2000 iterations per case. Details of the SIMPLEST algorithm [50,52] calculation procedures and the hybrid scheme [51] will not be repeated here.

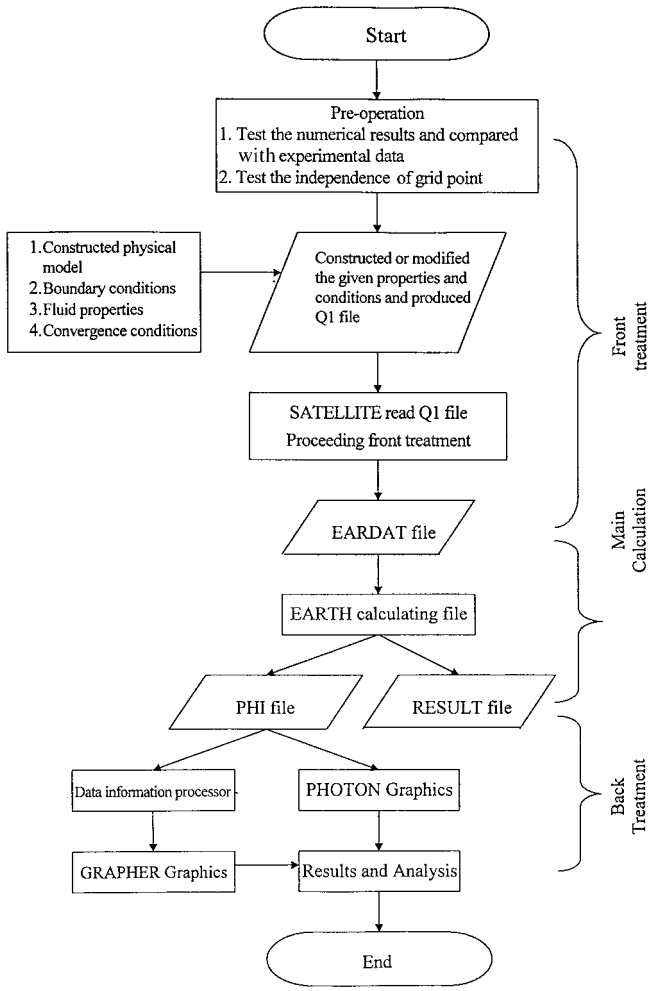

Figure 10. Flow chart of numerical simulation.

3.4. Boundary conditions

(a) At the inlet

$$u_i = V_j, \quad i = 1, 2$$

$$v = 0$$

$$w_i = V_j, \quad i = 1, 2$$

$$k_i = 0.003(V_j)_i^2, \quad i = 1, 2$$

$$\varepsilon_i = \frac{c_\mu k_i^{3/2}}{0.03(D_i/2)}, \quad i = 1, 2$$

(b) At the outlet

$$\frac{\partial \phi}{\partial x} = \frac{\partial \phi}{\partial y} = 0 \quad \text{and} \quad w = 0, \quad \phi = u, v, k, \varepsilon, p$$

(c) At the wall

$u = v = w = 0$ (no-slip condition), k and ε are handled by the wall function [12,51].

4. RESULTS AND DISCUSSION

The calculated results of velocity were compared with the experimental data of Barata *et al.* [42], as shown in Figure 11, under the same conditions and good agreement was found.

The velocity vector of upper and lower plates are shown in Plate 1. In order to see the distribution of velocity, the distance (z-axis) between the two plates is amplified eight times. Two strong main jet flows are injected downward from the nozzle, and induced the surrounding flow to enter the numerical simulation region. The flow direction of the fluid is spread into the surrounding when the twin-jet impinges the lower plate. The lower plate jet flow is formed

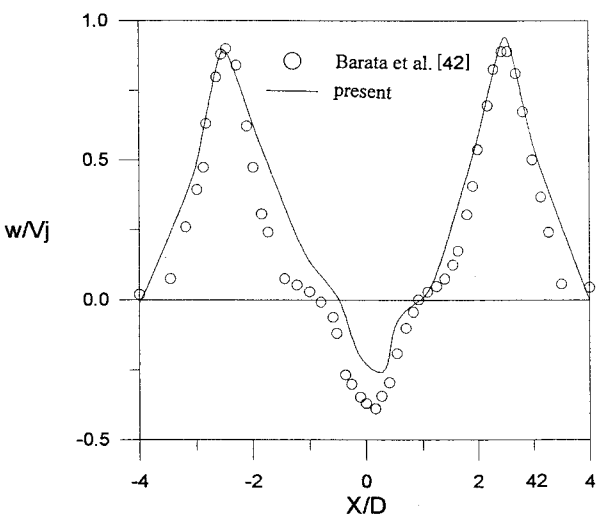

Figure 11. Mean velocity w of central line across two exhaust jets.

when the impinging flow is spread along the lower plate. The fountain up-wash region is formed between the inward flow of the lower plate jets due to the collided interaction, and the partial flow along the lower plate to the boundary is formed from a combined wall jet region. From the velocity vector distribution of the upper plate, we can see that the flow direction of the fountain up-wash flow between two impinging jets is upward. The upper wall jet regions are also formed when the fountain up-wash flow impinges the upper plate and changes the flow direction. Also, the recirculating zones are produced when the impinging flow of the upper plate interacts with the induced surroundings flow. The velocity vectors of three x–z cutted planes (A1–A1, A2–A2, A3–A3) are shown in Plate 2. The recirculation zones are clearly shown in Plate 2. Furthermore, the upper flow of fluid is formed from the inside region of the twin-jet extension to boundary. Therefore, the fountain up-wash region is not only narrowed and concentrated between twin jets, it is also extended to the boundary. The velocity vector of three y–z cutted planes (B1–B1, B2–B2, B3–B3) are shown in Plate 3. In order to view these, the length of the x-axis is amplified three times. The recirculation zones in the B2–B2 plane and the B3–B3 plane are clearly shown in Plate 3. The velocity vectors of eight cutted planes (vertical to the y-axis and along the positive z-axis) are shown in Figure 12. The flow along the parallel x-axis is stronger when the fluid flow is injected from the nozzle (cutted planes 4 and 5) due to the jet flow impinging the lower plate. The fluid flow along the parallel y-axis is stronger when the flow is located between twin jets, and the content of the combined region is a combined wall jet region or an upper wall jet region. The velocity vectors of eight cutted planes (vertical to the y-axis and along the negative x-axis) are shown in Figure 13. The maximum flow velocity along the positive z-axis appears at the cutted plane through two jet

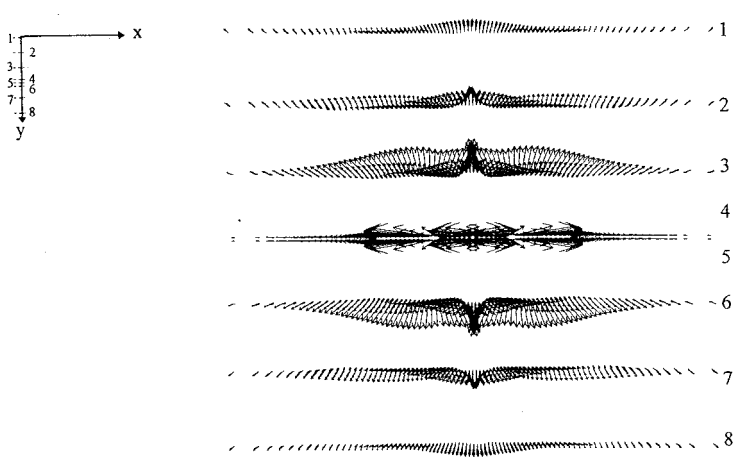

Figure 12. Mean velocity vector of cutted planes 1–8 (top view).

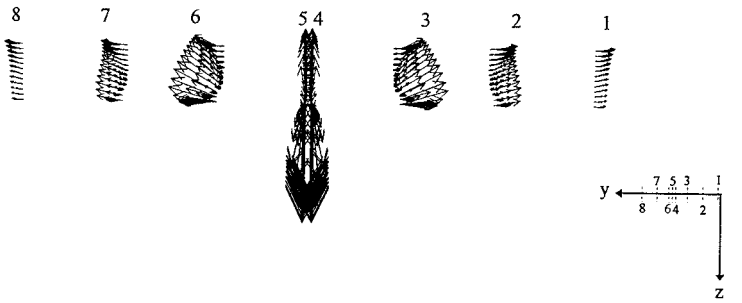

Figure 13. Mean velocity vector of cutted planes 1–8 (side view).

exits (cutted planes 4 and 5), i.e., through the main jet flow. From Figure 13, it can be seen that the flow velocity parallel to the y-axis is larger when it is near to the lower plate, because the initial velocity of the y component of the combined wall jet is larger than the upper wall jet (cutted planes 2, 3, 6, and 7). However, the results are incorrect when the flow is along the downward boundary (cutted planes 1 and 8) because the flow of upper plate parallel to the y-axis is formed by the fountain up-wash flow impinging the upper plate, and the flow of the lower plate parallel to the y-axis is formed by impinging between the lower wall jets and the spread to the surroundings.

The distribution of velocity vectors at various sub-layers of the x–y plane is shown in Figure 14(a)–(e). The recirculation phenomenon appears in every sub-layer of the x–y plane, and it gradually disappears nearer to the lower plate. The phenomenon of three-dimensional impinging jet flow is very complicated. The superposition recirculation zones of each plane can construct a three-dimensional phenomenon of the recirculation zone. From the side view of Figure 14, the downward flow of fluid (positive z-axis) is formed by the main jet and the induced flow of the surroundings. The upward flow (negative z-axis) is a fountain up-wash flow. Therefore, the larger upward velocity at various sub-layers appears in the regions between twin jets. From the front view of Figure 14, the fountain up-wash flow from the lower plate is more concentrated when it flows upstream. Then the flow is impinged and spread to surroundings until it approaches the upper plate. Further, the downward flow of the main jet also includes the spread fluid of fountain up-wash flow.

The distribution of velocity vectors in the x–y plane at a quarter of the various layers is shown in Figure 15(a)–(c). From the first layer of the x–y plane (neighboring the upper plate), it is obvious that two recirculation zones are formed due to the interaction between the upper wall jet flow and the induced flow. The total number of recirculation zones in the x–y plane is eight due to the symmetry of the flow. The recirculation zone is gradually spread when the height is decreased. Furthermore, the stronger upper wall jet region and the combined wall jet region become narrow and weak after the flow direction is left, as shown in Figure 15(c).

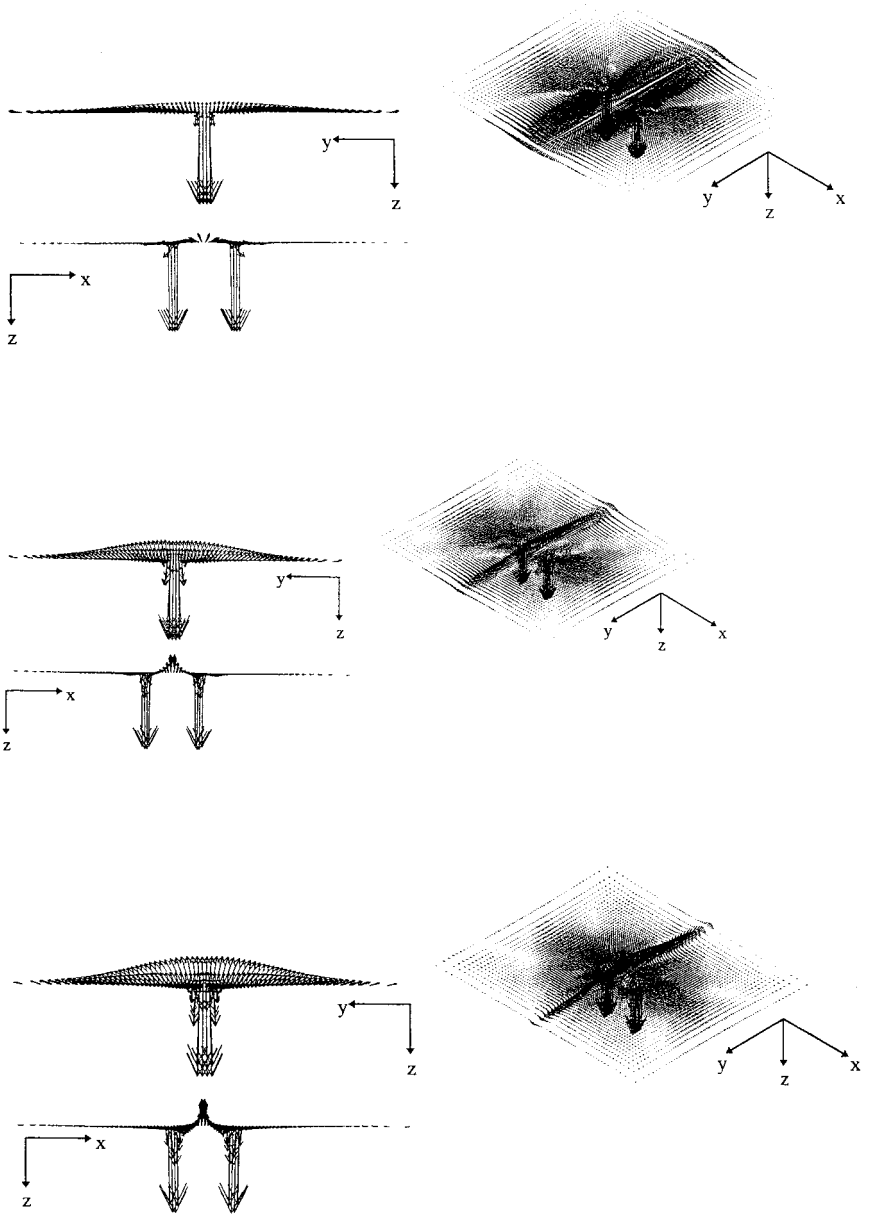

Figure 14. Mean velocity vector at various layers of the x–y plane. (a) First, (b) fourth, (c) seventh, (d) tenth, and (e) twelfth net grid layer of the z-axis.

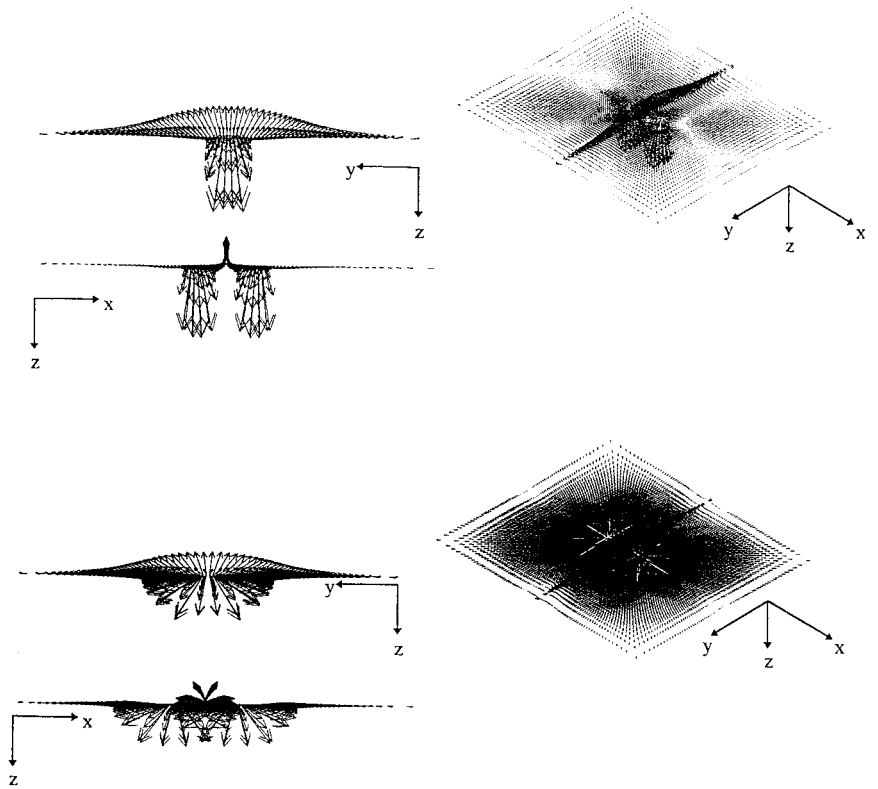

Figure 14 (*Continued*)

The u-, v-, w-, and p-contours, and the streamline of a cutted plane through two nozzles of the jet center are shown in Figures 16–19 respectively. The black line of a contour is a positive value and the colored line is a negative value. Ten contour lines are drawn between positive values and negative values. First, we can find the maximum gradient of the u-contour is located at the impinging jet region and the lower wall jet region because the fluid is turned and accelerated in the impinging region, as shown in Figure 16. The velocity of the lower wall jet is first accelerated and then decelerated because the pressure gradient of impinging jet region is larger. The initial acceleration of the impinging flow is from the stagnation point until the wall jet flow because the critical position is controlled by a viscous force. Similarly, the same condition appears in the fountain impingement region and the upper wall jet region. Furthermore, the gradient variation of the jet impingement region and the lower wall jet region is

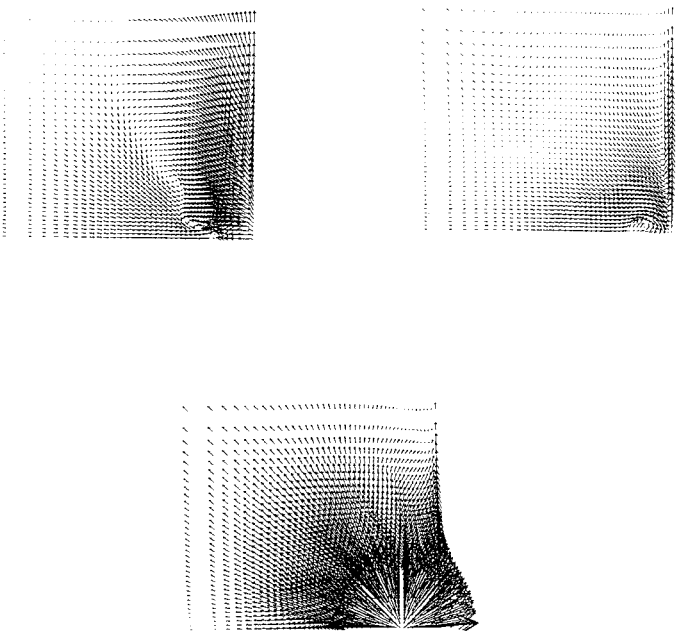

Figure 15. Mean velocity vector at various layers of a quarter of the x–y plane. (a) First, (b) eighth, (c) twelfth net grid layer.

larger than the above condition. The gradient variation of the u-velocity contour in the recirculation zone is also obvious.

The contour of the v-velocity is shown in Figure 17. From Figure 17, it is seen that the value of the v-velocity component is not large, but the gradient variation is obvious at the impingement region, the wall jet region, and the recirculation region. The w-velocity component contour of the central cutted plane is shown in Figure 18, and we find that the larger gradient variation appears in both sides of the main jets flow and the fountain up-wash flow. The pressure contour of the central cutted plane is shown in Figure 19. The maximum gradient variation of pressure is in the jet impingement region, as shown in Figure 19. The high pressure region also appears in the fountain formation region and the fountain impingement region. Also, the relative pressure of the recirculation zone is lower (the minimum relative pressure is at the recirculation center). The streamline of the central cutted plane is shown in Figure 20. The formation of the recirculation zone is shown in Figure 20.

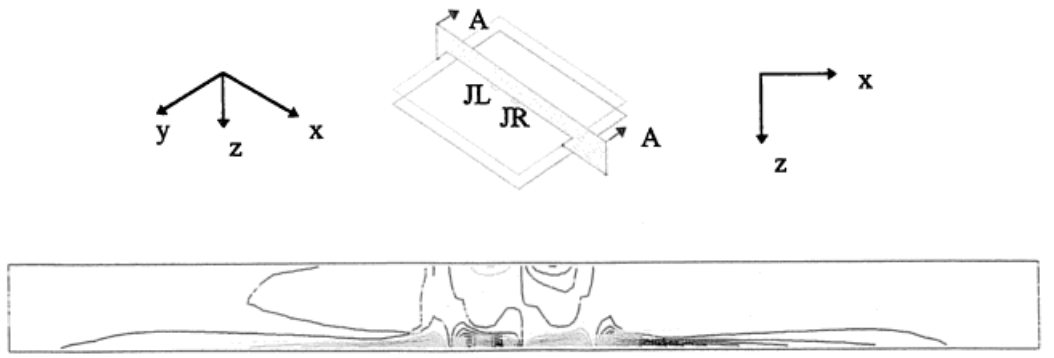

Figure 16. u-contours of the x–y plane across the central plane of two exhaust jets. Whole field range of values is from -9.77 to 9.77, the plane range of values is from -9.77 to 9.77 (no-crossflow, $\theta_L = 90°$, $\theta_R = 90°$, $S = 5D$, $H = 3D$, $Re = 105000$).

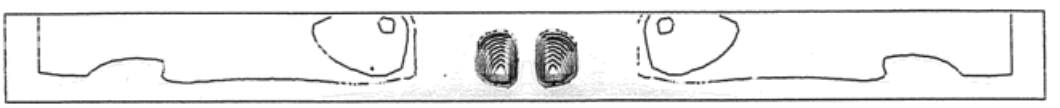

Figure 17. v-contours of the x–y plane across the central plane of two exhaust jets. Whole field range of values is from -9.06 to 9.06, the plane range of values is from -0.599 to 2.99 (no-crossflow, $\theta_L = 90°$, $\theta_R = 90°$, $S = 5D$, $H = 3D$, $Re = 105000$).

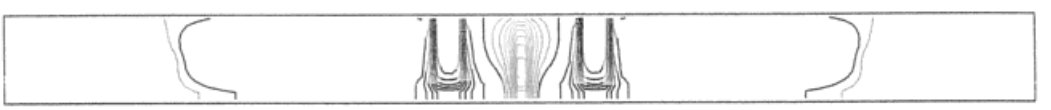

Figure 18. w-contours of the x–y plane across the central plane of two exhaust jets. Whole field range of values is from -5.45 to 16.3, the plane range of values is from -5.39 to 16.3 (no-crossflow, $\theta_L = 90°$, $\theta_R = 90°$, $S = 5D$, $H = 3D$, $Re = 105000$).

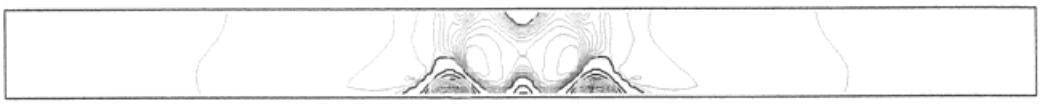

Figure 19. p-contours of the x–y plane across the central plane of two exhaust jets. Whole field range of values is from -10.5 to 125, the plane range of values is from -6.51 to 125 (no-crossflow, $\theta_L = 90°$, $\theta_R = 90°$, $S = 5D$, $H = 3D$, $Re = 105000$).

5. CONCLUDING REMARKS

A theoretical study has been undertaken to determine the flow characteristics associated with a three-dimensional turbulent incompressible impinging twin-jet with ground effect. The principal emphasis has been on gaining an understanding of the interaction of an impinging twin-jet flow on a simulated fuselage undersurface.

The calculated results show that the depth of the y-axis has a strong influence on the recirculation zone, the pressure distributions of the lower and upper plates, and on the lift of the flow. With the completion of a predictive scheme for the incompressible impinging jet, the analysis will be extended to multiple-jet three-dimensional flow problems using the PHOENICS code.

The three-dimensional impinging twin-jet flow treated in the present paper can be characterized by ten regions (see Section 1). The recirculation zones of three-dimensional impinging twin-jet flow with no-crossflow are produced from the upper plate. The recirculation zones are closed to the main nozzle jet and gradually spread over the ground surface when it is further up the upper plate. Such an analysis should provide a more detailed insight into the propulsion-induced flows around practical V/STOL aircraft.

APPENDIX A. NOMENCLATURE

C_1, C_2, C_μ	empirical constants in turbulence model
D	inlet width of exhaust nozzles
F	mass flow rate of control surface
H	height of jet exit plane above ground
J	total net flux of control surface
k	turbulent kinetic energy
P	static pressure
Re	Reynolds number
S	space of exhaust nozzles or source term
u	velocity component in the x-direction
v	velocity component in the y-direction

V_j exit velocity of nozzle jet
w velocity component in the z-direction

Greek letters

ε turbulent kinetic energy dissipation rate
ν_l molecular kinematic viscosity
ν_e effective kinematic viscosity
ν_t turbulent kinematic viscosity
Γ_ϕ effective transfer coefficient for diffusion

REFERENCES

1. Chuang SH. Numerical simulation of an impinging jet on a flat plate. *International Journal for Numerical Methods in Fluids* 1989; **9**: 1413–1426.
2. Chuang SH, Wei CY. Computations for a jet impinging obliquely on a flat surface. *International Journal for Numerical Methods in Fluids* 1991; **12**: 637–653.
3. Chuang SH, Chen MH, Lii SW, Tai FM. Numerical simulation of twin-jet impingement on a flat plate coupled with cross-flow. *International Journal for Numerical Methods in Fluids* 1992; **14**: 459–475.
4. Wolfshtein M. Some solutions of the plane turbulent impinging jet. *Journal of Basic Engineering*, *Transactions of the ASME* 1970; **92d**: 915–922.
5. Coleman DD. A study of free jet impinging. Part I: mean properties of free and impinging jets. *Journal of Fluid Mechanics* 1971; **45**: 281–316.
6. Parameswaran V, Alpay SA. Normal impingements of jets. *Journal of Aircraft* 1974; **11**: 189–191.
7. Sparrow EM, Lee L. Analysis of flow field and impingement heat/mass transfer due to a nonuniform slot jet. *Journal of Heat Transfer*, *Transactions of the ASME* 1975; **67c**: 191–197.
8. Siclari MJ, Migdal D, Palcza JL. The development of theoretical models for jet-induced effects on V/STOL aircraft. *Journal of Aircraft* 1976; **13**: 938–944.
9. Bower WW, Kotansky DR. A Navier–Stokes analysis of the two-dimensional ground effects problem. AIAA Paper 76-621, 1976.
10. Bower WW, Agarwal RK, Peters GR. A theoretical study of two and three dimensional impinging jets. MDRL Report 79-22, 1979.
11. Kotansky DR, Bower WW. A basic study of the VTOL ground effect problem for planar flow. *Journal of Aircraft* 1978; **15**: 214–221.
12. Jones WP, Launder BE. The prediction of laminarization with a two-equation model of turbulence. *Internationl Journal for Heat Mass Transfer* 1972; **15**: 301–314.
13. Rubel A. Computations of jet impingement on a flat surface. *AIAA Journal* 1980; **18**: 168–175.
14. Agarwal RK, Bower WW. Navier–Stokes computations of turbulent compressible two-dimensional impinging jet flowfields. *AIAA Journal* 1982; **20**: 577–584.
15. Looney MK, Walsh JJ. Mean-flow and turbulent characteristics of free and impinging jet flow. *Journal of Fluid Mechanics* 1984; **147**: 397–429.
16. Ho CM, Nosseir NS. Dynamiccs of an impinging jet. Part 1. The feedback phenomenen. *Journal of Fluid Mechanics* 1981; **105**: 119–142.
17. Rockwell D, Schachenmann A. Self-generation and organized waves in an impinging turbulent jet at low Mach number. *Journal of Fluid Mechanics* 1982; **117**: 425–441.
18. Ho CM, Nosseir NS. Dynamics of an impinging jet. Part 1. The noise generation. *Journal of Fluid Mechanics* 1982; **116**: 379–391.
19. Ho CM, Hsiao FB. Evolution of coherent structure in a lip jet. In *IUTAM Symposium on Structure of Complex Turbulent Shear Flow*, *Marseille*, *France*. Springer: Berlin, 1982; 121–136.
20. MacCormack RM. The effect of viscosity in hypervelocity impact cratering. AIAA Paper 69-354, 1969.
21. MacCormack RM. Computational efficiency achieved by time splitting of finite difference operators. AIAA Paper 72-154, 1972.
22. Beam RM, Warming RF. An implicit factored scheme for the compressible Navier–Stokes equations. *AIAA Journal* 1978; **16**: 393–402.

23. Pulliam TH, Steger JL. On implicit finite difference simulations of three dimensional flows. AIAA Paper 78-10, 1978.
24. Hwang CJ, Liu JL. Numerical study of two-dimensional impinging jet flowfields. *AIAA Journal* 1989; **27**: 841–842.
25. MacCormack RM. A numerical method for solving the equations of compressible viscous flow. AIAA Paper 81-0110, 1981.
26. Chuang SH, Cheng BJ. The block effects of an impinging twin-jet on a flat plate. In *Proceedings of the 1991 Aeronautics and Astronautics Conference*. The Aeronautical and Astronautical Society of the Republic of China: Taipei, 1991; 225–237.
27. Chuang SH, Chueng BJ, Chen MH. The transient hot flow analysis of an impinging twin-jet on a moving upper plate. In *Proceedings of the First National Conference on Computational Fluid Dynamics*. The Aeronautical and Astronautical Society of the Republic of China: Hsitou, 1992; 471–475.
28. Sung HM, Cheng BJ, Chuang SH. The effects of Reynolds number of twin-jet on V/STOL flow. In *Proceedings of the Symposium on Transport Phenomena and Applications*. Taipei, 1992; 129–136.
29. Chuang SH, Cheng BJ, Chen MH. The effect of cross flow on transient-state of impinging twin-jet with hot flow. In *Proceedings of the Ninth National Conference of the Chinese Society of Mechanical Engineering*. Kaohsiung, 1992; 73–80.
30. Chuang SH, Chang ZF. The block effect of an impinging twin-jet on a regular ground. Master Thesis of National Chuang-Hsing University, 1995.
31. Chuang SH, Lao MS. Hot flow of transient-state of twin-jet impingement on a regular ground. Master Thesis of National Chuang-Hsing University, 1996.
32. Miller P. A study of wall jets resulting from single and multiple inclined jet impingement. *Aeronautical Journal* 1995; **32**: 201–216.
33. Seyedein SH, Hasan M, Mujumdar AS. Turbulent flow and heat transfer from confined multiple impinging slot jets. *Numerical Heat Transfer* 1995; **18**: 35–51.
34. Donaldson CD, Snedeker RS. A study of free jet impingement. Part 1. Mean properties of free and impinging jets. *Journal of Fluid Mechanics* 1971; **45**: 281–319.
35. Siclari MJ, Hill Jr WG, Jenkins RC. Stagnation line and upwash formation of two impinging jets. *AIAA Journal* 1981; **19**: 1286–1293.
36. Kotansky DR, Glaze LW. Impingement of rectangular jets on a ground plane. *AIAA Journal* 1982; **20**: 585–586.
37. Elbanna H, Gahin S. Investigation of two plane parallel jets. *AIAA Journal* 1983; **21**: 986–991.
38. Barata JMM, Durao DFG, McGuirk JJ. Numerical study of single impinging jets through a crossflow. *Journal of Aircraft* 1989; **26**: 1002–1007.
39. Savory E, Toy N, McGuirk JJ, Sakellariou N. An experimental and numerical study of the velocity field associated with a jet in a crossflow. In *Engineering and Turbulence Modelling and Experiments*. Elsevier: Amsterdam, 1990; 165–173.
40. VanOverbeke TJ, Holdeman JD. Three-dimensional turbulent flow code calculation of hot gas ingestion. *Journal of Aircraft* 1990; **27**: 577–582.
41. Yoo S, Strash DJ. Zonal approach to V/STOL aerodynamics. *Journal of Aircraft* 1990; **27**: 866–871.
42. Barata JMM, Durao DFG, Heitor MV. Impingement of single and twin turbulent jets through a crossflow. *AIAA Journal* 1991; **29**: 595–602.
43. Lin YF, Sheu MJ. Interaction of parallel turbulent plane jets. *AIAA Journal* 1991; **29**: 1372–1373.
44. Lin YF, Lee YD, Teng JT. Experimental investigation of three-dimensional parallel twin-jet interaction. *Transactions of AASRC* 1995; **27**: 245–253.
45. Tafti DK, Vanka SP. Hot gas environment around STOVL aircraft in ground proximity—Part 2: numerical study. *Journal of Aircraft* 1992; **29**: 18–27.
46. Roth KR, Fearn RL, Thakur SS. Evaluation of Navier–Stokes prediction of a jet in a crossflow. *Journal of Aircraft* 1992; **29**: 185–193.
47. Kim SW, Benson TJ. Calculation of a circular jet in crossflow with a multiple-time-scale turbulence model. *International Journal for Heat Transfer* 1992; **35**: 2357–2365.
48. Kim SW, Benson TJ. Fluid flow of a row of jets in crossflow—a numerical study. *AIAA Journal* 1993; **31**: 806–811.
49. Özdemirc IB, Whitelaw JH. Impingement of an axisymmetric jet on unheated and heated flat plates. *Journal of Fluid Mechanics* 1992; **240**: 503–532.
50. Patankar SV. *Numerical Heat Transfer and Fluid Flow*. Hemisphere: New York, 1980.
51. Launder BE, Spalding DB. The numerical computation of turbulent flows. *Computer Methods in Applied Mechanics and Engineering* 1974; **3**: 269–289.
52. Patankar SV. A calculation procedure for two-dimensional elliptic situations. *Numerical Heat Transfer* 1981; **4**: 409–425.

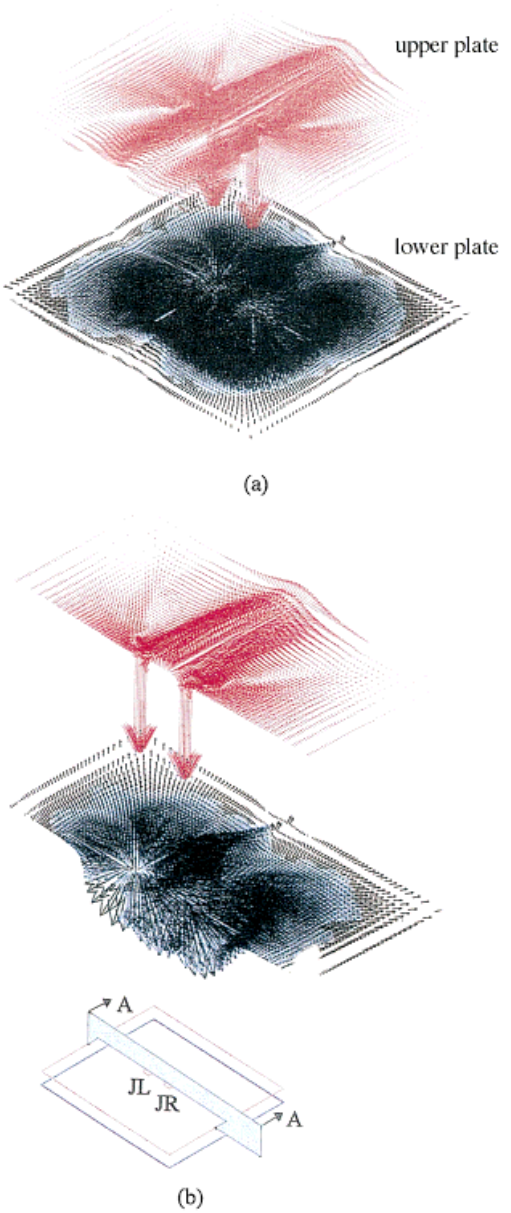

Plate 1. Mean velocity vector of upper and lower plates.

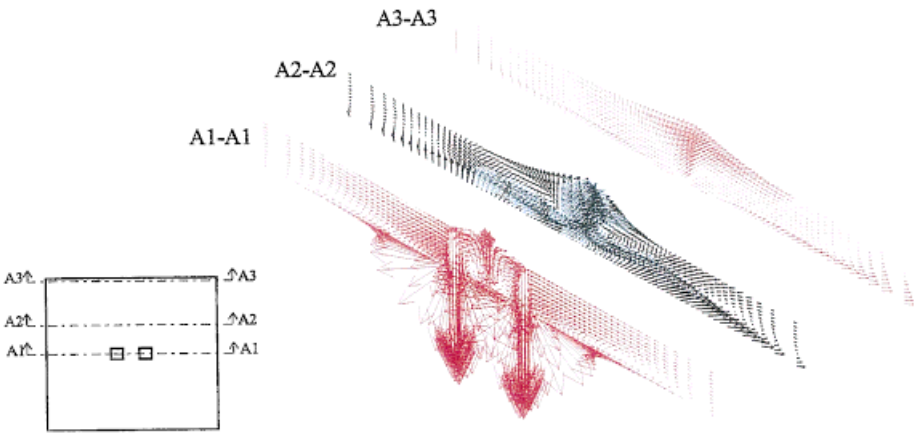

Plate 2. Mean velocity vector of cutted planes A1–A1, A2–A2, and A3–A3.

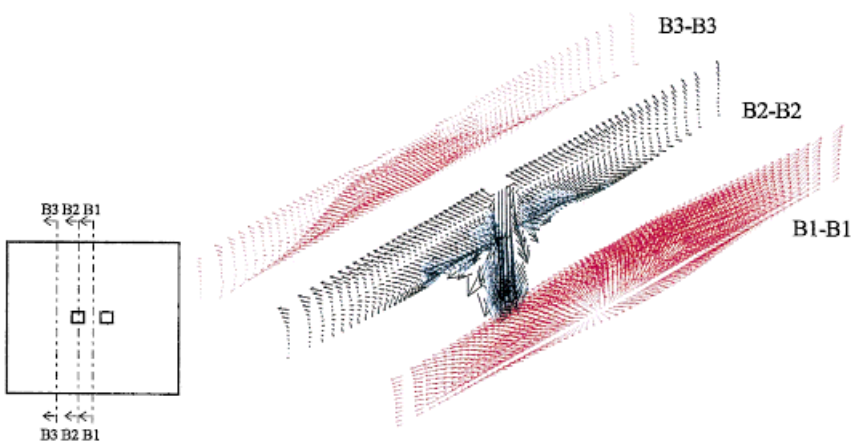

Plate 3. Mean velocity vector of cutted planes B1–B1, B2–B2, and B3–B3.